ELSEVIER

Chemical Engineering Journal 93 (2003) 91–101

Chemical Engineering Journal

www.elsevier.com/locate/cej

Combined methanol reforming for hydrogen generation over monolithic catalysts

B. Lindström, J. Agrell, L.J. Pettersson*

Department of Chemical Engineering and Technology, Chemical Technology, KTH—Royal Institute of Technology, SE-100 44 Stockholm, Sweden

Abstract

An experimental investigation on hydrogen generation from methanol using monolithic catalysts is presented in this paper. The activity and carbon dioxide selectivity for the reforming of methanol over various binary copper-based materials, Cu/Cr, Cu/Zn and Cu/Zr, have been evaluated. The methanol reforming was performed using steam reforming and combined reforming (CMR, a combination of steam reforming and partial oxidation). The CMR process was carried out at two modes of operation: near auto-thermal and at slightly exothermal conditions. The catalysts have been characterized using BET surface area measurement, X-ray diffraction (XRD), temperature programmed reduction (TPR) and scanning electron microscopy (SEM-EDS). The results show that the choice of catalytic material has a great influence on the methanol conversion and carbon dioxide selectivity of the reforming reaction. The zinc-containing catalyst showed the highest activity for the steam reforming process, whereas the copper/chromium catalyst had the highest activity for the CMR process. The copper/zirconium catalyst had the highest CO_2 selectivity for all the investigated process alternatives.

Keywords: Fuel cell vehicles; Methanol reforming; Hydrogen; Monoliths; Copper-based catalysts

1. Introduction

1.1. Fuel cell technology

Fuel cell technology is indisputably an ultra-clean method for generating electricity for mobile and stationary applications. The proton exchange membrane (PEM) fuel cell operates by electrochemical oxidation of hydrogen generating electricity while forming water (see Fig. 1). The fuel cell is highly sensitive to poisoning especially by carbon monoxide, which can significantly lower the performance of the fuel cell at concentrations above 50 ppm [1].

Providing the hydrogen required by the fuel cell to generate electricity is a challenging task associated with automotive fuel cell applications.

The hydrogen required by the fuel cell can either be stored in pressurized tanks, as metal hydrides or produced on-board from a liquid fuel with high hydrogen content. Storing pure hydrogen on-board is unsuitable due to the limited driving range and logistical complications associated with refueling the pressurized tanks. The cost of revamping the gasoline tanks to operate with an alternative liquid fuel is also considerably lower than for a pressurized gas.

Catalytic conversion of liquids with high hydrogen to carbon ratio, such as primary alcohols, is possible at relatively low temperatures (200–300 °C) and sought of by the automotive industry as one of the most promising solutions for generating the hydrogen on-board the automobile.

Methanol is today the primary candidate, as hydrogen carrier, for the on-board production of hydrogen, due to its high hydrogen to carbon ratio (4:1), low boiling point and availability. The absence of carbon–carbon bonds in methanol drastically reduces the risk of coking. Methanol can also be produced from renewable resources and thus lowering the production of greenhouse gases.

1.2. Methanol reforming

Hydrogen production from methanol is possible through several process alternatives: decomposition, steam reforming (SR), partial oxidation (PO) and combined reforming (CMR) [2].

Thermal or catalytic decomposition (Eq. (1)) is the most simple conversion method as only methanol is used in the feedstock [3].

$$CH_3OH(g) \rightarrow 2H_2 + CO, \qquad \Delta H^\circ = 90.7\,\text{kJ/mol} \qquad (1)$$

The decomposition of methanol yields a product gas containing up to 67% hydrogen and 33% carbon monoxide. The

* Corresponding author. Tel.: +46-8-790-8259; fax: +46-8-10-85-79.
E-mail address: larsp@ket.kth.se (L.J. Pettersson).

1385-8947/02/$ – see front matter
PII: S1385-8947(02)00112-2

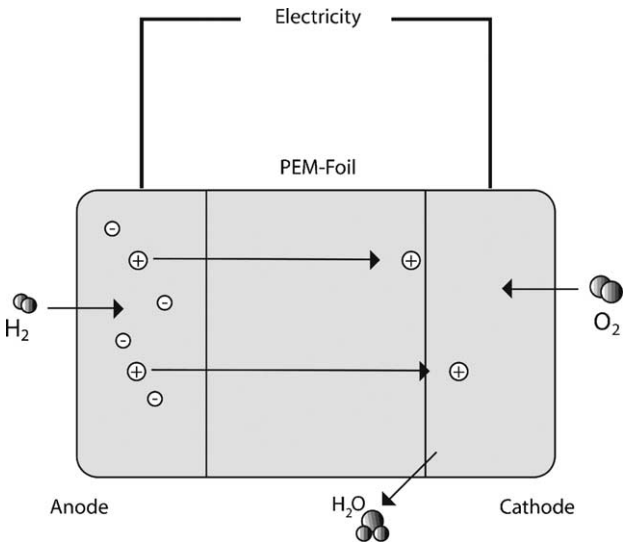

Fig. 1. Fuel cell schematic.

production of carbon monoxide makes the process unsuitable as the compound has detrimental effects on the performance of the fuel cell, which was reported in the previous section. The reaction is also highly endothermic which can cause problems in mobile applications where energy supply is scarce.

The steam reforming process (Eq. (2)) has received much attention [4–6] due to the ability to produce a gas with high hydrogen concentration, up to 75%, while maintaining a high selectivity towards carbon dioxide. The main drawback of steam reforming is that the reaction is endothermic and slow.

$$\mathrm{CH_3OH(g) + H_2O(g) \rightarrow 3H_2 + CO_2},$$
$$\Delta H^\circ = 49.5\,\mathrm{kJ/mol} \quad (2)$$

Partial oxidation (Eq. (3)) is a fast and exothermic reaction [7–9]. When applying the partial oxidation process, it is possible to construct compact and highly responsive systems.

For partial oxidation of methanol it is possible to achieve a product stream with hydrogen concentrations up to 67% when using pure oxygen in the feed.

However, for automotive solutions the required oxygen would most likely be supplied from air, diluting the product gas with nitrogen. In such a system the maximum theoretical hydrogen content is lowered to 41%. The hydrogen concentration is directly linked to the fuel cell's ability to utilize the incoming hydrogen. At low concentrations mass transfer limits the reaction rate and thus the amount of hydrogen converted to electricity is lowered [10].

$$\mathrm{CH_3OH(g) + \tfrac{1}{2}O_2 \rightarrow 2H_2 + CO_2},$$
$$\Delta H^\circ = -192.3\,\mathrm{kJ/mol} \quad (3)$$

The highly exothermic nature of the partial oxidation process can cause the formation of hot spots in the reactor, which can cause catalyst deactivation through sintering.

The choice of conversion process is directly linked to the intended application. For automotive solutions small and highly responsive systems are desired which can quickly adjust to changes in flow conditions, caused by transients during acceleration and changes in driving conditions. The system's ability to supply a clean product gas containing a high hydrogen concentration is vital for the performance of the fuel cell vehicle.

A system based upon partial oxidation can fulfil the criteria linked with size and speed, however, it is not possible to achieve satisfactory hydrogen concentrations. Steam reforming on the other hand delivers a slow system with high hydrogen concentrations, thus, neither of the processes are on their own suited for automotive applications.

Combining partial oxidation and steam reforming processes can result in a process, which can deliver relatively high hydrogen concentrations at moderate response rates, as well as avoiding the formation of hot spots. The exact nature and performance of the CMR system is dependent on the steam to oxygen ratio at which the CMR reaction is carried out (Eq. (4)). CMR is sometimes referred to as oxidative steam reforming or auto-thermal reforming, when operated under adiabatic conditions [11,12].

$$\mathrm{CH_3OH(g) + (1-}p\mathrm{)H_2O(g) + \tfrac{1}{2}}p\,\mathrm{O_2 + 1.9N}p_2$$
$$\rightarrow \mathrm{CO_2 + (3-}p\mathrm{)H_2 + 1.9N}p_2,$$
$$\Delta H^\circ = 49.5 - 241.8p \quad (4)$$

The variable p in Eq. (4) is the stoichiometric factor for the CMR system, representing the steam to oxygen ratio. When p is zero Eq. (4) is reduced to the SR reaction and when p equals 1 the reaction is reduced to the PO reaction. The overall heat of reaction is strongly dependent on the value of p, which directly influences the thermal properties of the CMR system.

Increasing the oxygen/steam ratio will increase the exothermic nature of the CMR reaction, while lowering the maximum theoretical hydrogen concentration. Steam and combined reforming are commonly operated with an excess of steam, 20–30%. The excess steam is mainly present in order to reduce the carbon monoxide content in the effluent by inducing the water-gas shift (WGS) reaction in the reformer (Eq. (5)). The PEM fuel cell also requires humid conditions [10], which can be supplied by operating the reformer in this manner.

$$\mathrm{CO + H_2O(g) \rightarrow H_2 + CO_2},$$
$$\Delta H^\circ = -41.2\,\mathrm{kJ/mol} \quad (5)$$

The WGS reaction reduces the carbon monoxide content while increasing the hydrogen content in the product stream and low temperatures favor the forward reaction at equilibrium conditions [13].

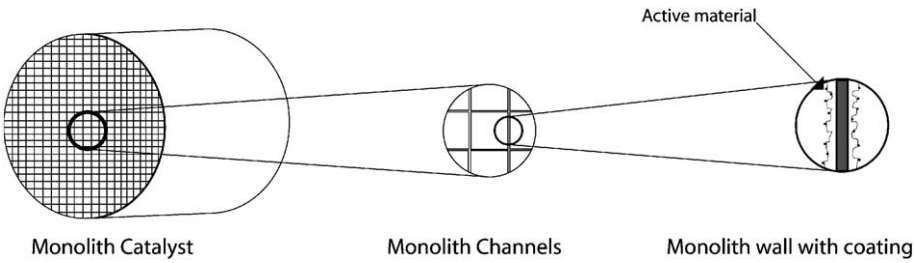

Fig. 2. Schematic view of the construction of a monolith.

1.3. Monoliths as catalyst substrates

The automotive environment is harsh due to mechanical stress, caused by vibrations, and constant alterations of the operating conditions. The catalyst used in this type of application must, therefore, be exceptionally robust. Methanol reforming has traditionally been performed over pellet catalysts, which may not be suitable for vehicular applications as they are easily mechanically destroyed by attrition.

Ceramic monoliths have been used with great success as exhaust gas catalysts and are accepted by the automotive industry as stable substrates [14]. Monoliths are uniform extruded structures composed of parallel flow-through channels and are usually based upon ceramic materials or aluminium containing metals (see Fig. 2).

The ceramic substrate used in automotive catalysts is coated with a high surface area inorganic oxide, i.e. γ-Al_2O_3, upon which the active material is dispersed [15]. Monoliths have high open frontal area and, hence, a very low pressure drop compared to packed beds. For endothermic reactions, such as steam reforming, the use of monoliths can be problematic as heat transfer is poor between the channels, due to the low heat conductivity of the ceramic material. The use of partial oxidation or combined reforming (operating under exothermic conditions) is more suitable as heat can be transferred axially through each channel and, thus, obtaining an even temperature distribution.

One obvious disadvantage with monolithic catalysts is their lower content of active material per unit reactor volume. This implies that it is important to prepare the catalyst in such a way that the active phase is highly active [16]. A high loading, a high dispersion and a uniform active phase distribution are desired.

The Reynold's number will decrease substantially in a monolith channel compared to in a fixed bed. Consequently, due to the laminar flow both heat and mass transfer characteristics are influenced in a negative way. There is no mass transfer in the radial direction between channels, which decreases the conversion. Some of these drawbacks can be addressed by using for example segmented monoliths.

In these experiments, we have chosen copper-based materials, as they were highly active in previous tests using pellets [17], for investigating the feasibility of using monoliths for automotive reforming.

2. Experimental

2.1. Catalyst preparation

The cordierite ($2MgO \times 5SiO_2 \times 2Al_2O_3$) monolith substrate was initially coated with aluminum oxide (γ-Al_2O_3), to increase the surface area and to enable dispersion of the catalytic material. The γ-Al_2O_3 powder (see Table 1 for material data) was suspended in ethanol and ball milled for 24 h prior to coating the monolith. The monolith was then dipped into the γ-Al_2O_3 slurry and dried for 1 h at 120 °C. The procedure was repeated until 15 wt.% γ-Al_2O_3 had been deposited on the monolith.

The active materials (see Table 2), all in the form of nitrates, were dissolved in water and the pH kept above the iso-electric point of γ-Al_2O_3. The metal salts were mixed in fixed weight ratios (see Table 2) and the γ-Al_2O_3 coated monoliths were dipped in the metal nitrate solutions. The monoliths were then dried at 120 °C for 2 h and calcined at 350 °C for 5 h. The metal loading of each monolith was 10 wt.% of the washcoat including active material.

2.2. Catalytic activity

The catalytic material was tested in a tubular reactor operating at atmospheric pressure. The reactants were fed to

Table 1
Material data

Material	Data	Manufacturer
Ethanol (C_2H_5OH)	99.5 vol.% spectroscopic	Kemetyl
Alumina (γ-Al_2O_3)	Surface area 150 g m^{-2}	Condea
Monolith	Cordierite 400 cpsi	Corning
$Cu(NO_3)_2^* \times H_2O$	M_w: 241.5 g mol^{-1}	Alfa Aesar
$Cr(NO_3)_3^* \times H_2O$	M_w: 400 g mol^{-1}	Alfa Aesar
$Zn(NO_3)_2^* \times H_2O$	M_w: 297 g mol^{-1}	Merck
$ZrO(NO_3)_2^* \times H_2O$	M_w: 231.2 g mol^{-1}	Alfa Aesar

Table 2
Catalyst composition

Catalyst	Composition (wt.%)	Active material (wt.%)
CuZn	40:60	10.2
CuCr	40:60	10.1
CuZr	40:60	10.3

Table 3
Operating conditions

Operating condition	O_2/H_2O	p[a]	ΔH° (kJ mol^{-1})[b]
Steam reforming	0	0	49.5
Near auto-thermal	0.125	0.2	1.14
Combined reforming	0.214	0.3	−23.0

[a] Stoichiometric factor for combined reforming.
[b] Calculated from formula given in Eq. (4).

the reactor with 30% excess steam in order to lower CO concentrations by inducing the WGS reaction.

Prior to each experiment the catalyst was reduced in a 10% H_2 in N_2 mixture at a heating rate of 5 °C min^{-1} and dwelling at 220 °C for 2 h. The product stream composition was measured on-line using a gas chromatograph from Varian equipped with both TCD and FID detectors. The experiments were carried out over a temperature interval of 180–300 °C, where the temperature is measured outside the axial entrance of the monolith. The reactor was made of stainless steel (ASTM 316) with an inner diameter of 25 mm. For all experiments a space velocity (SV) of 10,000 h^{-1} was used. Three monoliths of the following size were used in series: 22 mm in diameter and 20 mm in length.

The catalysts were tested for three different operating conditions: steam reforming, combined reforming at near auto-thermal operating conditions and combined reforming under slightly exothermic conditions. Details of the operating conditions are listed in Table 3.A detailed schematic of the laboratory test system is presented in Fig. 3.

2.3. X-ray diffraction

The crystal phases were identified by means of X-ray powder diffraction (XRD) using a Siemens Diffractometer 5000. The operating parameters were: monochromatic Cu Kα radiation, Ni filter, 30 mA, 40 kV, 2θ scanning from 10 to 90°, and a scan step size 0.02. Phase identification was done using the reference database (JCPDS-files) supplied with the equipment.

2.4. Scanning electron microscopy

The catalyst samples were analyzed using a Zeiss DSM 940 scanning electron microscope (SEM) equipped with a QX2000 energy dispersive X-ray spectrometry (EDS) unit.

2.5. BET surface area measurements

The specific surface area of the various samples was measured according to the Brunauer–Emmett–Teller theory (BET) by nitrogen adsorption using a Micrometrics ASAP 2010 instrument. Prior to adsorption measurements, the samples were degassed for at least 12 h at 250 °C.

2.6. Temperature programmed reduction

Temperature programmed reduction (TPR) experiments were carried out using a Micromeritics TPD/TPR 2900 instrument. Fresh calcined samples of approximately 25 mg were subjected to a stream of 10% H_2 in Ar flowing at 90 cm^3 min^{-1} and increasing the temperature at 10 °C min^{-1}. The current of the thermal conductivity detector was maintained at 50 mA and the detector temperature kept constant at 100 °C.

3. Results

3.1. Catalytic activity measurements

The catalysts were tested for steam reforming (SR), combined reforming (CMR) at near auto-thermal operating conditions (CR1) and CMR under exothermal operating conditions (CR2). For details on the catalyst make-up and the relationship between oxygen and methanol consult the section on experimental work. The results are presented as volumetric concentrations of hydrogen (H_2), carbon dioxide (CO_2), carbon monoxide (CO) and CO_2 selectivity (S_e). The equation used to derive the CO_2 selectivity (S_e) is described in Eq. (6). All concentrations presented in this paper have been compensated for the presence of inert nitrogen.

$$S_e(\%) = \frac{CO_2}{CO_2 + CO} \times 100 \quad (6)$$

The results show that CO was the main by-product formed in the reforming process. This agrees well with the reaction mechanisms proposed by Amphlett and co-workers [4,6].

The results presented are divided into two sections, process comparison and material evaluation.

3.1.1. Process comparison

In this section, the effect on the catalytic activity by varying the operating conditions, is shown for the individual catalysts.

The response of the copper/zinc (Cu/Zn) catalyst to variations in the oxygen/steam ratio is shown in Fig. 4a,b. The hydrogen yield obtained from the different processes is dependent on the oxygen/steam ratio, where the best results are achieved when using the CR2 process and lowest for the SR. This result can be explained by the fact that the heat transfer occurs axially and that the oxygen is initially consumed by partial oxidation generating heat in the direction of flow. The SR reaction, which is strongly endothermic, results in a temperature drop in the beginning of the reactor lowering the reaction rate, thus, explaining why higher hydrogen yields are obtained for the oxidative processes compared to the steam reforming process. The CR1 reaction yields the highest H_2 values at temperatures >290 °C, which can be coupled to the lower theoretical maximum hydrogen content in the CR2 reaction when the steam reforming part of the

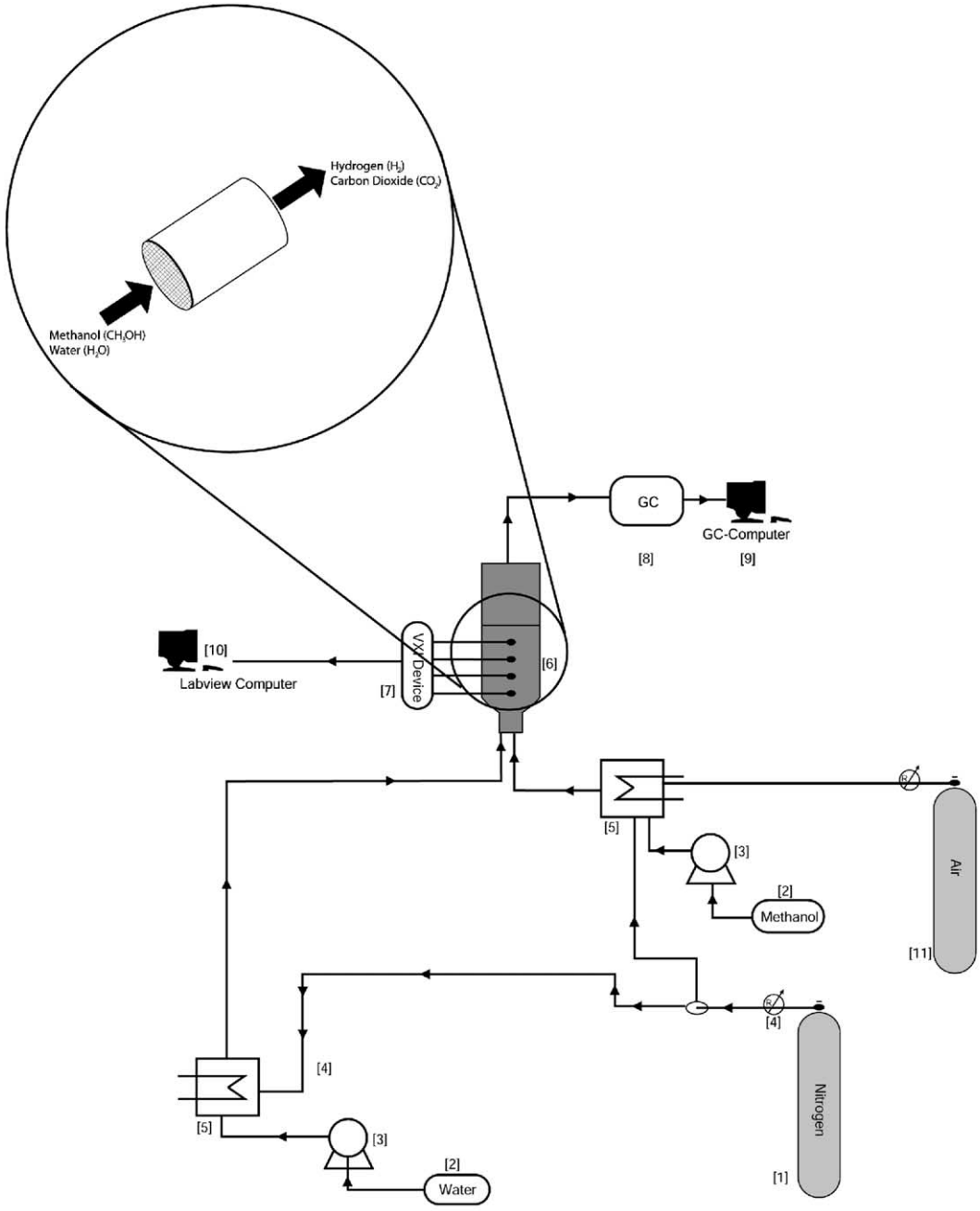

Equipment Description

1:Carrier gas (99.999 % Nitrogen AGA)
2:Fuel Tanks (Deionized water and 99.9 % Methanol)
3:Pumps (Braun Perfusor)
4:Mass flow controller (Bronkhorst HI-TEC)
5:Evaporators
6 :Flow reactor
7 :Thermocouple module (National Instruments)
8 :Varian Gas Chromatograph (FID & TCD detectors)
9 :Computer with GC evaluation software
10:Computer with Labview for temperature measurement
11:Oxygen supply (Air AGA)

Fig. 3. Laboratory reactor system.

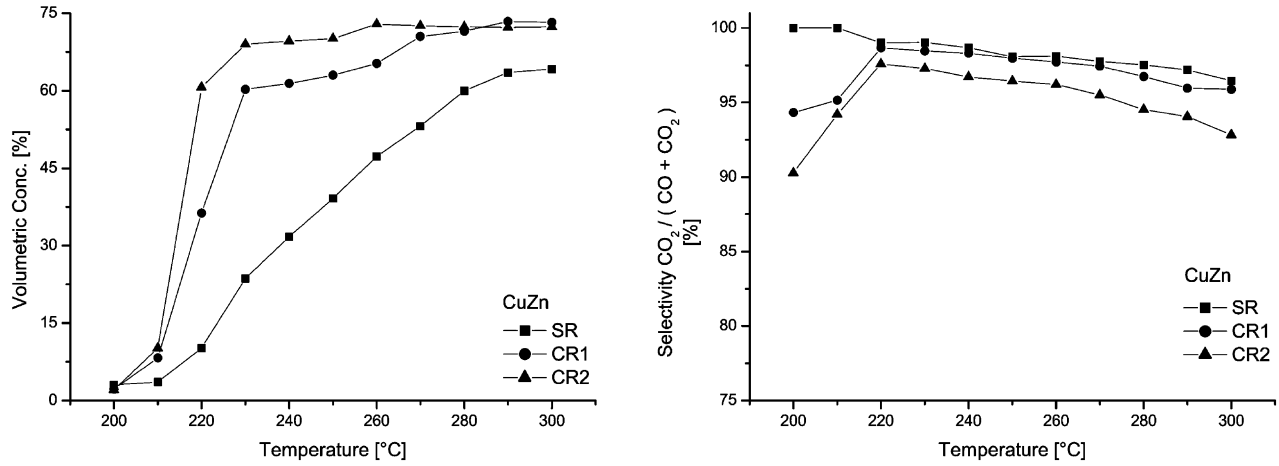

Fig. 4. (a) Hydrogen concentration; (b) carbon dioxide selectivity.

Table 4
Copper/zinc catalyst

Process	H_2 (210 °C, vol.%)	H_2 (max, vol.%)	T (60% H_2, °C)	S_e[a] (min, %)	S_e[a] (mean, %)	CO (max, vol.%)
SR	3.6	64.2	280	96.5	98.3	0.77
CR1	8.26	73.4	230	94.3	97.0	1.07
CR2	10.6	72.3	220	90.3	95.1	1.75

[a] S_e: carbon dioxide selectivity.

CMR system operates efficiently. The carbon dioxide (CO_2) selectivity is highest for the SR reaction and lowest for the CR2 reaction (see Fig. 4b), where a maximum CO content of 1.7 vol.% is obtained (see Table 4).

The copper/chromium (Cu/Cr) catalyst follows the same trends as the Cu/Zn catalyst with the highest H_2 yields (see Fig. 5a) obtained when using the CR2 process. However, the difference in yield between CR1 and CR2 is lower and the CR1 reaction gives higher H_2 concentrations above 260 °C. The gap between the SR reaction and the CMR processes is also larger for the Cu/Cr catalyst compared to the Cu/Zn.

The trend of the CO_2 selectivity (see Fig. 5b) is inversed compared to Cu/Zn, and the best results are obtained for the CR2 reaction. The highest CO value (see Table 5), 2.5 vol.%, is obtained when using the CR1 process.

The zirconium-containing catalyst (Cu/Zr) behaves slightly different in all processes obtaining similar H_2 concentrations for temperatures <225 °C (see Fig. 6a), where the highest concentrations were obtained by the SR reaction. For temperatures 230 and 270 °C the highest yields were obtained by the CR2 reaction while >270 °C the CR1 reaction is the most efficient process. The CR1 process

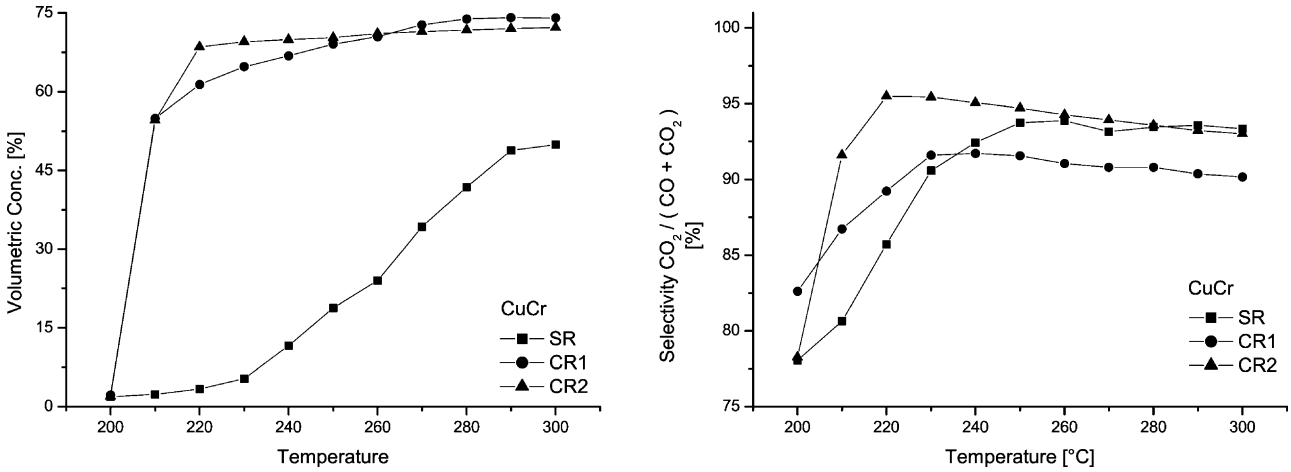

Fig. 5. (a) Hydrogen concentration; (b) carbon dioxide selectivity.

Table 5
Copper/chromium catalyst

Process	H_2 (210 °C, vol.%)	H_2 (max, vol.%)	T (60% H_2, °C)	S_e[a] (min, %)	S_e[a] (mean, %)	CO (max, vol.%)
SR	2.3	49.9	–	78	89.8	1.13
CR1	54.5	74.1	220	82.6	89.7	2.50
CR2	54.4	72.2	215	90.3	78.3	1.79

[a] S_e: carbon dioxide selectivity.

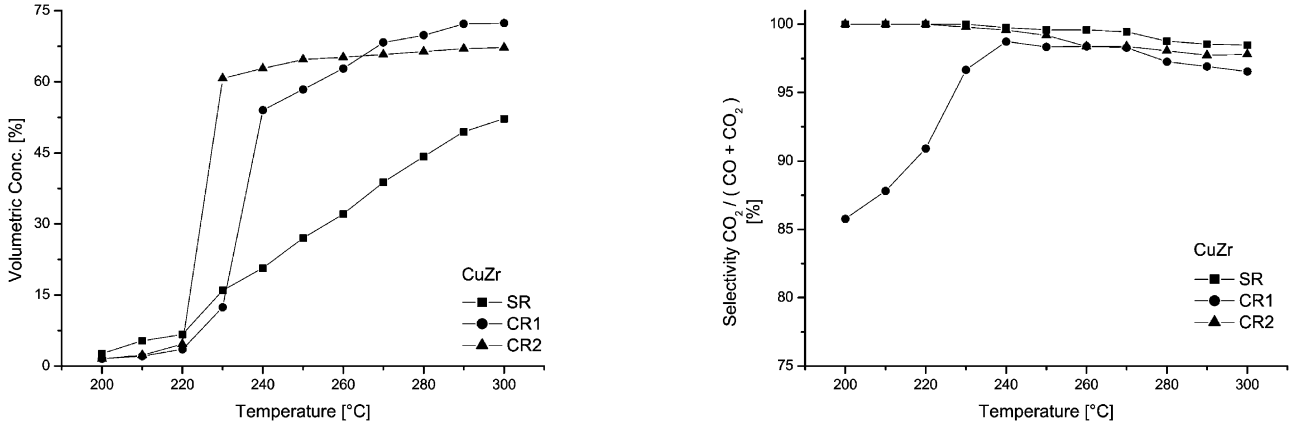

Fig. 6. (a) Hydrogen concentration; (b) carbon dioxide selectivity.

achieves the absolute highest hydrogen concentration. The zirconium-containing catalyst achieves the best CO_2 selectivity when using the SR process, 95%, and the lowest mean value (see Table 6) is obtained when running the CR1 reaction. The highest CO concentrations, 0.87%, for the zirconium catalyst were obtained when running the CR1 process at 300 °C.

3.1.2. Material evaluation

In this section, we compare the catalytic materials under the various operating conditions. The effect of the endothermic nature of the steam reforming (SR) process is evident with all three materials showing low activity (see Fig. 7a) at temperatures below 230 °C. For the SR process the Cu/Zn catalyst is the most active catalyst with respect to the generation of hydrogen, while the Cu/Zr catalyst achieves slightly superior results compared to the Cu/Cr catalyst. The hydrogen concentration did not exceed 65% for any of the catalysts. The mean carbon dioxide (CO_2) selectivity (see Fig. 7b) for steam reforming were highest for the Cu/Zr containing catalyst and the lowest selectivity was obtained when using the chromium catalyst (see Table 7), which also gave the absolute highest CO concentration (0.53%).

For CMR at near auto-thermal operating conditions (CR1) the Cu/Cr catalyst was superior for the entire temperature span (see Fig. 8a) with hydrogen concentrations above 70%. The zirconium-containing catalyst generated the lowest hydrogen yields over the entire temperature interval and was only able to produce hydrogen concentrations >60% at 250 °C compared to 220 °C for the chromium catalyst. The CO_2 selectivity of Cu/Cr was low, as in the case of the SR process, with absolute CO concentrations of 2.5% at 300 °C. The Cu/Zr catalyst showed the highest CO_2 selectivity (see Fig. 8b) for the CR1 process.

For the CMR under exothermal conditions (CR2) the chromium-containing catalyst gave the highest hydrogen concentrations (see Fig. 9a) at temperatures below 230 °C. However, above 230 °C the Cu/Zn catalyst performed as well as the Cu/Cr catalyst with respect to the generation of H_2. The Cu/Zr catalyst gave the highest mean CO_2 selectivity values for the CR2 process and the Cu/Cr catalyst again showed the lowest CO_2 selectivity.

Table 6
Copper/zirconium catalyst

Process	H_2 (210 °C, vol.%)	H_2 (max, vol.%)	T (60% H_2, °C)	S_e[a] (min, %)	S_e[a] (mean, %)	CO (max, vol.%)
SR	2.7	52.2	–	98.4	99.5	0.27
CR1	2.10	72.3	252	85.7	95.1	0.84
CR2	2.30	67.2	230	97.7	98.9	0.51

[a] S_e: carbon dioxide selectivity.

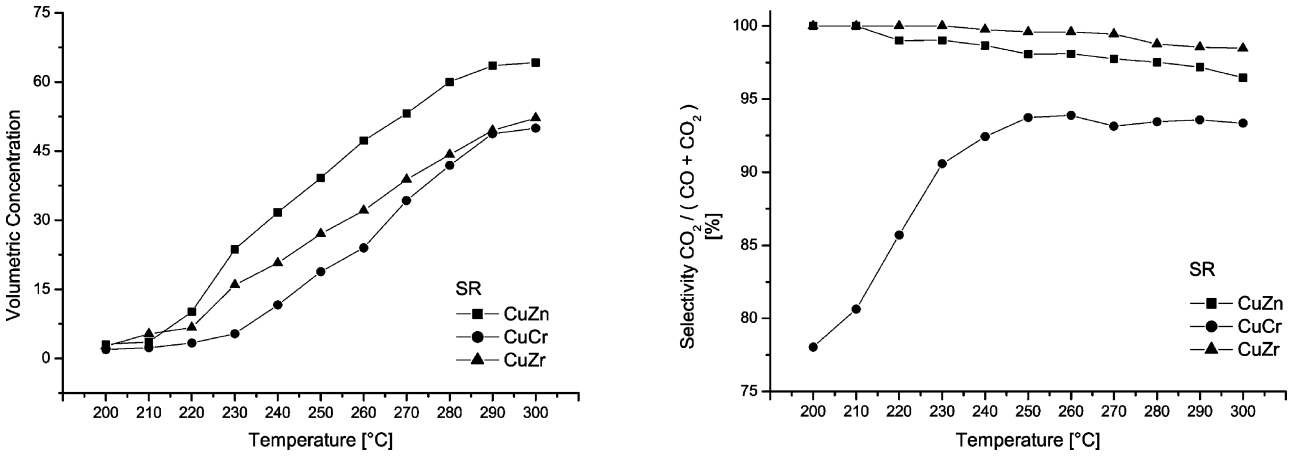

Fig. 7. (a) Hydrogen concentration; (b) carbon dioxide selectivity.

Table 7
Comparison of hydrogen generation processes

Catalyst	Process	H_2 (210 °C, vol.%)	H_2 (max, vol.%)	T (60% H_2, °C)	S_e[a] (min, %)	S_e[a] (mean, %)	CO, (max, vol.%)
Cu/Zn	SR	3.6	64.2	280	96.5	98.3	0.77
Cu/Cr	SR	2.3	49.9	–	78.0	89.8	1.13
Cu/Zr	SR	2.7	52.2	–	98.4	99.5	0.27
Cu/Zn	CR1	8.3	73.4	230	94.3	97.0	1.07
Cu/Cr	CR1	54.5	74.1	220	82.6	89.7	2.5
Cu/Zr	CR1	2.10	72.3	252	85.7	95.1	0.84
Cu/Zn	CR2	10.6	72.3	220	90.3	95.1	1.75
Cu/Cr	CR2	54.4	72.2	215	90.3	78.3	1.79
Cu/Zr	CR2	2.30	67.2	230	97.7	98.9	0.51

[a] S_e: carbon dioxide selectivity.

3.1.3. Summary of activity results

The highest CO_2 selectivity for all process was obtained when using the zirconium-containing catalyst and the lowest for the chromium catalyst. For the steam reforming (SR) process the zinc-containing catalyst gave the highest hydrogen yields whereas for the CMR processes (CR1 and CR2) the chromium catalyst gave the highest yields. The SR process gave the overall lowest hydrogen concentrations for all of the tested catalysts. For high temperatures the CR1 process gave the highest hydrogen concentrations for all catalysts.

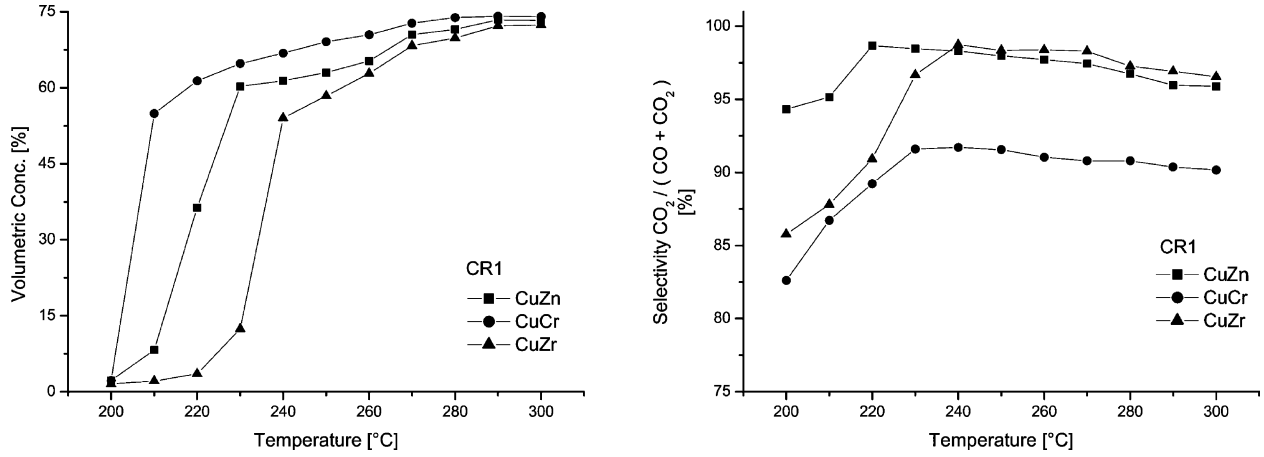

Fig. 8. (a) Hydrogen concentration; (b) carbon dioxide selectivity.

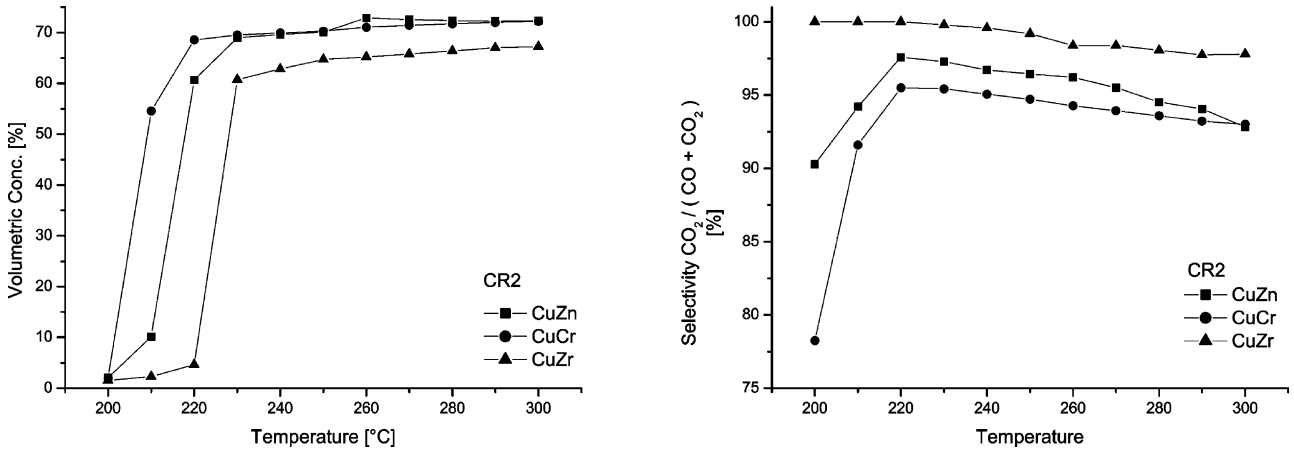

Fig. 9. (a) Hydrogen concentration; (b) carbon dioxide selectivity.

3.2. Catalyst characterization

Fig. 10 shows the X-ray diffractograms obtained on the copper-containing catalysts. The XRD spectra were collected after calcination at 350 °C. For the Cu/Zn catalyst the Cu and Zn existed as separate oxides (CuO and ZnO). The Cu/Cr catalyst existed as a mixed oxide ($CuCrO_4$). The Cu/Zr catalyst existed as separate oxides in the same manner as the Cu/Zn catalyst. The aluminum oxide was for all cases in the gamma phase. The mixed structure of the Cu/Cr catalyst is a possible explanation for the high affinity of the catalyst for oxidation and low affinity for the steam reforming (SR) process contrary to the zinc and zirconium-based catalysts.

SEM-EDS was used to investigate how the active materials were dispersed on the aluminum oxide surface. The results obtained indicate that for the case of the Cu/Zn and Cu/Cr catalyst that the Cu/Zn and Cu/Cr are merged together on the surface. For the chromium-based catalyst this result was expected as the copper and chromium was found as a mixed oxide by the XRD. For the zirconium-based catalyst the copper crystallites were found to be smaller than the zirconium crystallites and dispersed over the entire surface around single Zr particles. The different surface structure of the Zr-based catalyst, compared to the zinc and chromium-based, is a possible explanation for the lower CO contents obtained when using the Cu/Zr catalyst.

The surface areas obtained from the BET measurements were fairly similar (see Table 8) with the highest area acquired from the zirconium-based catalyst.

Table 8
Surface area for alumina-supported catalysts

Catalyst	Surface area (BET, $m^2\,g^{-1}$)
Cu/Zn	104
Cu/Cr	95
Cu/Zr	127

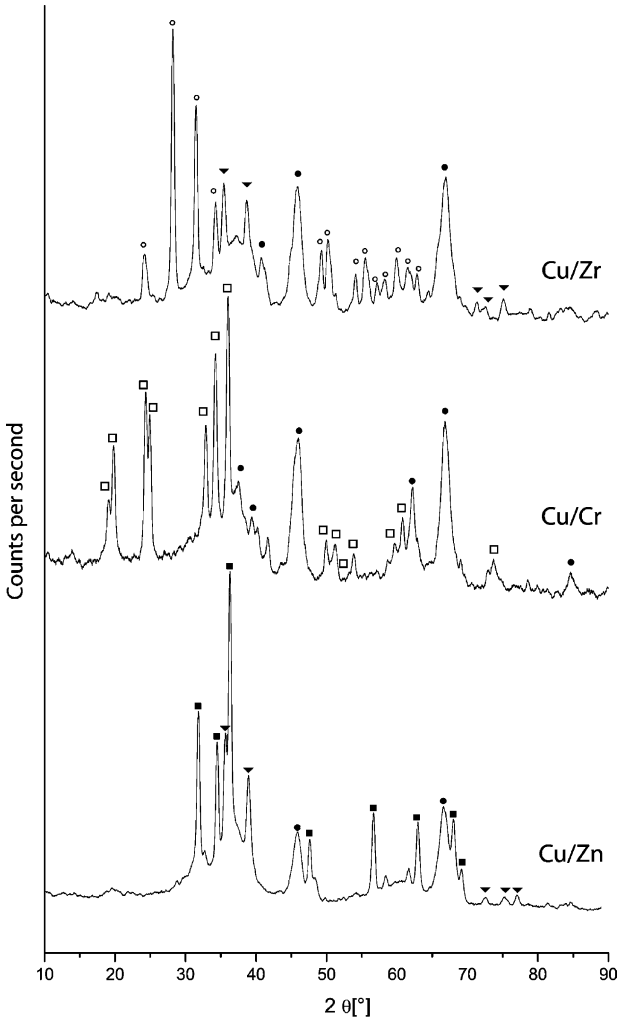

Fig. 10. X-ray diffraction spectra: ZnO (■), Al_2O_3 (●), CuO (▼), ZrO_2 (○), and $CuCrO_4$ (□).

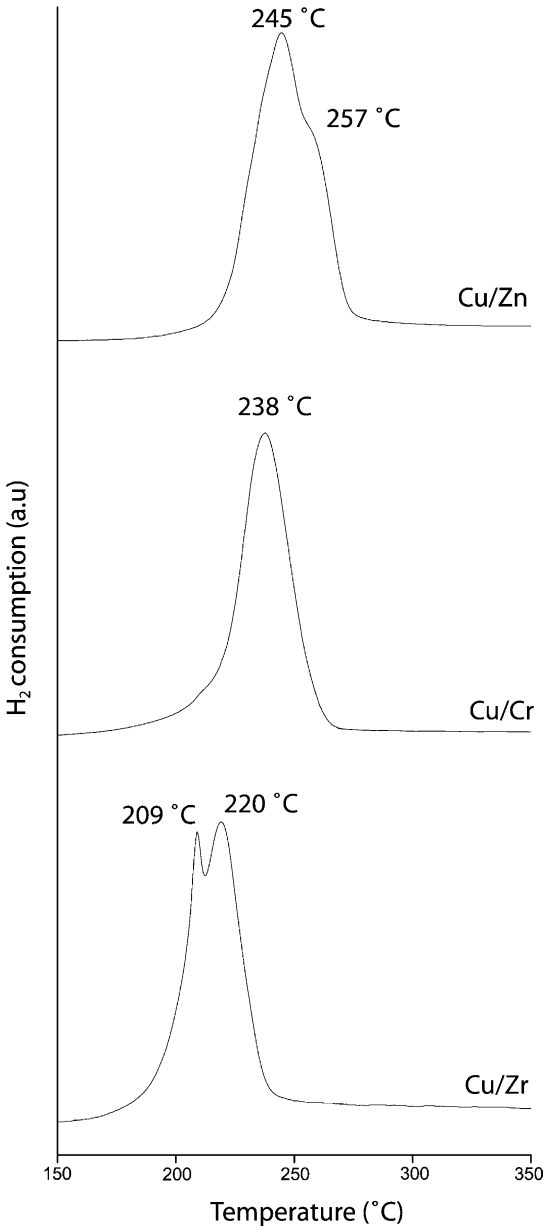

Fig. 11. Temperature programmed reduction profiles.

The results from temperature programmed reduction of the fresh Cu/Zn, Cu/Cr and Cu/Zr catalysts are shown in Fig. 11. All features are attributed to reduction of copper oxide, forming metallic copper and water ($CuO + H_2 \rightarrow Cu^0 + H_2O$).

The reduction profile of the Cu/Zn catalyst displays a first peak at 245 °C and a shoulder at about 257 °C. The consumption of hydrogen is initiated at around 200 °C, and completed at 280 °C. The shoulder may be attributed to the stepwise reduction of copper oxide ($Cu^{2+} \rightarrow Cu^{+} \rightarrow Cu^0$), which could indicate a strong interaction between part of the copper and zinc oxide in the sample. The Cr-containing catalyst displays a narrower peak than its Zn-containing counterpart, indicating a narrower particle size distribution. Furthermore, reduction is initiated at a lower temperature, about 180 °C, suggesting that the CuO particles are smaller and better dispersed than in the Cu/Zn sample. The peak reaches a maximum at 238 °C and reduction is complete at about 270 °C. Reduction of the Cu/Zr catalyst begins at the lowest temperature observed for the three samples, close to 160 °C. The width at half peak-height is narrower than that observed for the Cu/Zn catalyst, but broader than that of the Cu/Cr catalyst, indicating a somewhat broader copper particle size distribution than in Cu/Cr. Two maxima are observed, appearing at 209 and 220 °C. Reduction is completed at about 250 °C, indicating that this sample possesses the highest copper dispersion of the analyzed catalysts. This correlates well with the results from the SEM and BET analyses (see above).

4. Conclusions

Methanol reforming over monolith-based catalysts shows great potential for on-board hydrogen generation. The materials and operating conditions greatly affect conversion and carbon dioxide selectivity. We tested copper catalysts with three different promoters, chromium, zinc and zirconium, for steam reforming, combined reforming at near auto-thermal operating conditions and at exothermal operating conditions. For steam reforming the highest conversion was obtained for the zinc-containing catalyst whereas for the oxidative process the chromium-containing catalyst gave the highest conversions. The zirconium catalyst generated the lowest carbon monoxide concentration under all operating conditions. For catalysts yielding CO concentrations >1% a low temperature shift step must be implemented prior to the clean-up step, which is undesirable in automotive applications as the available space is limited. Complete methanol conversion is not obtained under any operating conditions tested in the experiments and, thus, the amount of catalyst used limits the reaction.

The use of steam reforming is clearly limited in automotive applications, as large amounts of heat must be supplied for the process to meet the required methanol conversion. The combined methanol reforming processes on the other hand have great potential for methanol reforming over monoliths.

Acknowledgements

The authors gratefully acknowledge financial support from Volvo Technological Development Corporation, the Swedish Energy and KTH-Royal Institute of Technology.

References

[1] T.J. Schmidt, H.A. Gasteiger, R.J. Behm, J. Electrochem. Soc. 146 (1999) 1296.
[2] J. Agrell, B. Lindström, L.J. Pettersson, S.G. Järås, Catalytic hydrogen generation from methanol, in: J.J. Spirey (Ed.), Catalysis—

Specialist Periodical Reports, Royal Society of Chemistry, Cambridge, vol. 16, pp.67–132.
[3] L. Pettersson, K. Sjöström, Combust. Sci. Tech. 80 (1991) 265.
[4] J.C. Amphlett, R.F. Mann, B.A. Peppley, D.M. Stokes, in: Proceedings of the 26th Intersociety Energy Conversion Engineering Conference, 1991, p. 642.
[5] J.P. Breen, J.R.H. Ross, Catal. Today 51 (1999) 521.
[6] B.A. Peppley, J.C. Amphlett, L.M. Kearns, R.F. Mann, Appl. Catal. A 179 (1999) 21.
[7] M.L. Cubeiro, J.L.G. Fierro, Appl. Catal. A 168 (1998) 307.
[8] S. Velu, K. Suzuki, T. Osaki, Catal. Lett. 62 (1999) 159.
[9] J. Agrell, K. Hasselbo, K. Jansson, S.G. Järås, M. Boutonnet, Appl. Catal. A 211 (2001) 239.
[10] J. Larminie, A. Dicks, Fuel Cell Systems Explained, Wiley, Chichester, UK, 2000.
[11] S. Golunski, Platinum Met. Rev. 42 (1998) 2.
[12] R. Kumar, S. Ahmed, M. Krumpelt, Electric Hybrid Veh. Technol. 96 (1996) 123.
[13] M.V. Twigg (Ed.), Catalyst Handbook, 2nd Edition, Wolfe Publishing Co., London, 1989.
[14] K.C. Taylor, CHEMTECH 20 (1990) 551.
[15] R.M. Heck, S. Gulati, R.J. Farrauto, Chem. Eng. J. 82 (2001) 149.
[16] T. Vergunst, F. Kapteijn, J.A. Moulijn, Appl. Catal. A 213 (2001) 179.
[17] B. Lindström, L.J. Pettersson, Int. J. Hydrogen Energy 26 (2001) 923.